This is the peer-reviewed, final accepted version for American Mineralogist, published by the Mineralogical Society of America.
The published version is subject to change. Cite as Authors (Year) Title. American Mineralogist, in press.
DOI: https://doi.org/10.2138/am-2022-8584. http://www.minsocam.org/

Magnetic Contributions to Corundum-Eskolaite and Corundum-Hematite Phase Equilibria: a DFT Cluster Expansion Study

Daniel J. Pope[1], Aurora E. Clark[1], Micah P. Prange[2], and Kevin M. Rosso[2]

[1]Department of Chemistry, Washington State University, Pullman, Washington 99164, USA

[2]Pacific Northwest National Laboratory, Richland, Washington 99532, USA

May 7, 2022

Abstract

Magnetic contributions have the potential to significantly influence predicted phase stability within alloy and mineral mixing phase diagrams, yet have been historically challenging to incorporate due to a significant increase to phase space sampling. In this work, we employ a computational protocol that includes spin orientation as an additional configurational component within multi-component cluster expansions between magnetic and non-magnetic metal oxide alloys (calculated using density functional theory (DFT) and the generalized gradient approximation). This approach was used to determine the effect of magnetic contributions to corundum-eskolaite and corundum-hematite phase equilibria from first principles.

Two-component cluster expansions of the magnetic components of eskolaite and hematite were first performed showing the ability of this method to properly calculate their respective magnetic properties. Two-component cluster expansions were then performed for non-magnetic Al(III) and ferromagnetic Cr(III) and Fe(III), and phase diagrams were calculated for later comparison. Finally, a non-magnetic Al(III) and "up" and "down" magnetic configuration for anti-ferromagnetic Cr(III) and Fe(III) were performed. Magnetic contributions to the calculated phase diagram for the corundum-eskolaite system was shown to be inconsequential, but is absolutely vital for accurate determination of the corundum-hematite solvus.

This is the peer-reviewed, final accepted version for American Mineralogist, published by the Mineralogical Society of America.
The published version is subject to change. Cite as Authors (Year) Title. American Mineralogist, in press.
DOI: https://doi.org/10.2138/am-2022-8584. http://www.minsocam.org/

Introduction

Corundum-eskolaite, α-(Al,Cr)$_2$O$_3$ and corundum-hematite, α-(Al,Fe)$_2$O$_3$ phase equilibria have been extensively researched in experimental studies(Jacob (1978); Sitte (1985); Chatterjee et al. (1982); Atlas & Sumida (1958); Turnock & Eugster (1962); Feenstra et al. (2005)), but little work has been done to describe these solid-solutions from first principle calculations.(Pinney et al. (2009); Chatterjee et al. (2016); Eremin et al. (2008)) This is perhaps due to additional complexity introduced by magnetic degrees of freedom present in both the Cr(III) and Fe(III) cations and the difficulty required to accurately calculate these contributions. More accurate modeling of these magnetic properties and their influence on phase equilibria would allow for better understanding of the underlying phenomena governing these systems and make predictive finite temperature structures more accessible for further study.

Corundum, hematite, and eskolaite are isostructural R-3c space group minerals that are important compounds in the production of many industrial materials. Additionally, hematite and eskolaite both exhibit unique magnetic properties making them of high interest for a multitude of spintronics applications.(Pattanayak et al. (2021); Khan et al. (2015); Borisov et al. (2005); He et al. (2010)) Alloy composition is often a guiding factor in material design of these systems, and accurate simulations of alloy compositions are highly desirable.

Prior computational work for both systems has been confined to ab initio energy calculations of dilute limit substitutions(Chatterjee et al. (2016)) and pair configurations(Pinney et al. (2009)) within moderately sized supercells or from classical molecular dynamics free energy calculations yielding associated phase equilibria diagrams.(Eremin et al. (2008)) While the MD simulations provide complete solvus line calculations, they rely on interaction potentials using fitted parameters to better model thermodynamics. Presently, to the authors' knowledge, there are currently no complete first-principle solvus line calculations for these systems.

Accurate determination of phase equilibria in alloys is typically performed through Cluster Expansion (CE) calculations(Sanchez et al. (1984)), where ensemble average free energies can be determined rapidly and used to create phase diagrams. This method normally examines atomic configurations only, e.g. A B site configurations in binary alloys, but can be extended to capture magnetic effects as well. This is achieved through a multi-component cluster expansion,(Van De Walle (2009)) where "up" and "down" magnetic moments at each spin polarized cation site is included as an additional configurational component. This approach may be essential for the eskolaite and hematite systems since they are both anti-ferromagnetic at low temperatures and capturing these low energy states are essential for determining mixing energies.

This approach, however, can result in missing intermediate energy microstates, lowering the magnetic entropy. As a result, while this approach improves phase diagram calculations through the inclusion favorable anti-ferromagnetic pair interactions, it overestimates the stability of these phases resulting in greatly increased

magnetic disordering temperatures. These missing states can be included through methods in which magnetic moments are treated with constant magnitude and variable direction during Monte Carlo finite temperature calculations allowing for estimation of Heisenberg-like spin-spin interaction energies.(Lavrentiev et al. (2010); Garrity (2019)), but this is not readily available in current cluster expansion computational packages. Additionally, due to this, finer features of the phase diagram due to interaction between magnetic and chemical ordering(Burton (1991)) would not be accurately modeled in these calculations.

It is important to note that CE requires a series of ab initio calculations of the alloy configurations in order to obtain interaction energies. Thus they are somewhat limited in that more computationally expensive hybrid functionals are impractical to implement. For transition metal oxides and magnetic systems, use of other functionals, e.g. GGA's, often require careful implementation of Hubbard U parameters to correctly describe magnetic interactions.(Shi et al. (2009); Rollmann et al. (2004)) However tuning this parameter does provide a means in which to lower magnetic pairing energies, thereby artificially matching the expected magnetic disordering properties. This will also affect atomic interactions as well though, so the effect of tuning this parameter on the resulting phase diagrams typically needs to be examined.

Toward this end, we implement this multi-component cluster expansion by examining the mixing properties of corundum-eskolaite and corundum-hematite. As we demonstrate, the relative impact of including the magnetic contributions to the corundum-eskolaite and corundum-hematite alloy to the calculated phase diagrams may be significant. The computational protocol is outlined in the Theory and Methodology section and is first verified by determination of the known lattice and magnetic properties of the pure systems of hematite and eskolaite. To formulate a basis for comparison, corundum-hematite and corundum-eskolaite phase diagrams were first calculated assuming a ferromagnetic orientations only. These systems were then recalculated now including the additional magnetic degrees of freedom and the resulting shifts in the calculated phase diagrams are presented. While a more complete picture of the calculated phase diagram would also include vibrational contributions, inclusion of these effects and their possible interactions with the magnetic contributions is beyond the scope of this work.

Theory and Methodology

The corundum-eskolaite and corundum-hematite systems represent an alloy mixture of a non-magnetic (NM) Al and magnetic (M) Cr or Fe metal ion. Treatment of the magnetic contributions as a configurational state of either an "up" or "down" collinear magnetic moment results in a ternary phase diagram comprised of NM, M↑, and M↓ components as represented in Fig 1.

This is the peer-reviewed, final accepted version for American Mineralogist, published by the Mineralogical Society of America.
The published version is subject to change. Cite as Authors (Year) Title. American Mineralogist, in press.
DOI: https://doi.org/10.2138/am-2022-8584. http://www.minsocam.org/

Solid solution phase diagrams can be calculated given that the energy of any random alloy configuration is known. This is achieved through the thermodynamic integration of the semi-grand-canonical ensemble of alloy configurations with respect to temperature and chemical potential.(van de Walle & Asta (2002)) In order to simulate an ensemble of configurations requires rapid estimation of any given alloy configuration energy. This can be achieved through multi-component cluster expansions in the form of Eq. 1, where E is the energy of some configuration σ, α is a cluster, m_α are multiplicities of clusters with equivalent symmetry, and J_α is the Effective Cluster Interaction (ECI) energy. The terms inside the angle brackets represent the cluster correlation functions, which are averaged over all clusters symmetry equivalent to α. Details of this equation are given more completely in other work.(Van De Walle (2009))

$$E(\sigma) = \sum_{\alpha} m_\alpha J_\alpha \langle \prod_i \gamma_{\alpha_i, M_i}(\sigma_i) \rangle_\alpha \tag{1}$$

The primary task in a cluster expansion calculation is to truncate the complete cluster expansion basis to some finite sum that is predictive of new configurations. This is achieved by fitting the Effective Cluster Interaction term, J_α, to a series of energies of different configurations calculated by ab initio methods. New alloy configurations can now be rapidly calculated and used for statistical sampling and generation of alloy phase diagrams. In this study, cluster expansion calculations are separated into three configurational categories; purely magnetic, atomic, and atomic plus magnetic. For each category, cluster expansions were performed. In Sec. **Properties of Eskolaite and Hematite**, we first examine the individual magnetic properties of eskolaite and hematite using CE. The magnetism of eskolaite and hematite are well known, and the initial goal is to ensure that cluster expansion methods will accurately capture their magnetic properties validating further use within multi-component systems. These were performed using M↑ and M↓ lattice site configurations. The purely magnetic configurations were also calculated over a series of DFT+U values. Adjusting this parameter will affect the strength of magnetic interactions as well as the cohesive energy of the crystal. Both of these effects will ultimately influence the final calculation of alloy phase diagrams, and would ideally be set to values satisfying accuracy in both instances.

In Sec. **Configurational Phase Boundary of Corundum-Eskolaite and Corundum-Hematite**, cluster expansions are performed using NM and M↑ lattice site configurations only, and binary phase diagrams were calculated. Both eskolaite and hematite are normally anti-ferromagnetic, but this methodology restricts the magnetic species to higher energy ferromagnetic states only. This provides a simplified first approximation with which to first compare to experimental data, and to examine how introducing magnetic degrees of freedom

affects the resulting phase diagram calculations.

In Sec. **Configurational and Magnetic Contributions to Phase Boundary of Corundum-Eskolaite and Corundum-Hematite**, the configurational plus magnetic system is determined by the construction of a 4-component cluster expansion. For example, the corundum-eskolaite system consists of a series of labeled chemical components Cr1, Cr2, Al3, Al4. Here the Cr1 is a M↑ component and the Cr2 is a M↓ component. The aluminum components lack a magnetic moment, but are separated into two identical cluster expansion components in order to yield the correct compositional high temperature statistics. For example, at the high temperature limit for equiatomic composition, there should be an equal number of Cr and Al atoms. Without including a second, but identical, aluminum component, the high temperature limit would give an equal probability of occupying a lattice site by either a Cr1, Cr2, or a single Al, leading to over representation of Cr. This ultimately leads to a quaternary, instead of the ternary phase diagram picture in Fig. 1, but can be projected into a final binary phase diagram between the total Cr and Al components.

This approach allows for the correction of the ground state energy of an anti-ferromagnetic system, which is improperly modeled as ferromagnetic in the binary configurational system. It also allows for the inclusion of the magnetic disordering transition in the free energy landscape, which may shift the purely configurational phase boundary in unpredictable ways. The disordering temperature, can represented by Eq. 2, and demonstrates that it can be shifted up or down depending on the strength of the change in magnetic energy or entropy upon going from an ordered phase a, to a disordered phase b.

$$T^{a\to b}_{config+mag} = \frac{\Delta U^{a\to b}_{config} + \Delta U^{a\to b}_{mag}}{\Delta S^{a\to b}_{config} + \Delta S^{a\to b}_{mag}} \tag{2}$$

The major drawback of this method is the inclusion of only the two magnetic states, which artificially heightens the magnetic disordering temperature. However, the magnitude of the difference between configurational plus magnetic system vs. just the binary configurational system would at least be informative of the possible importance of this effect.

Computational Details

The crystal structure used is isomorphic between corundum, eskolaite, and hematite and is described using the rhombohedral primitive unit cell of space group $R-3c$. Electronic structure calculations were performed using the Vienna ab-initio simulation package (VASP)(Kresse & Furthmüller (1996)) within the framework of plane-wave density functional theory in periodic boundary conditions. Projector Augmented Wave (PAW)(Kresse & Joubert (1999)) methods were employed to represent the core electron energies using VASP POTCAR v5.4

PAWs. Due to the large number of calculations required for determination of ECIs, the exchange correlation is represented by the computationally inexpensive generalized gradient approximation (GGA+U) using the Perdew, Burke, and Ernzerhof (PBE)(Perdew et al. (1996)) variant.

DFT+U was added using the VASP implementation of the Dudarev method(Dudarev et al. (1998)). The Hubbard J value was kept constant at 0 eV, and the Hubbard U value was adjusted relative to J. A value of U equal to 0 eV represents the absence of the DFT+U correction. U-J Hubbard correction values of J = 0 and of U = 0 through 5 eV were used to compare lattice properties of the eskolaite and hematite systems. From these, it was found that a U = 0 eV value for eskolaite and U = 2 eV value for hematite best described overall properties which are detailed further in the results section.

The plane wave basis energy cutoff for all structures was converged to energy differences of less than 1 meV per 50 eV increase. For all systems, the maximum required energy cutoff, 900 eV, was used across all systems to ensure accurate energy comparisons. To avoid Pulay stress error,(Francis & Payne (1990)) the energy cutoff was increased by 30% for all geometry optimizations. A static calculation at the original cutoff was then performed to obtain the total energy. Brillouin zone sampling was performed with gamma-centered k-points using the Monkhorst-Pack scheme(Pack & Monkhorst (1977)) and again converged to energy differences within 1 meV for all unit cell crystal structures with a k-point mesh of $4\times4\times4$. All supercell structures were sampled inversely proportional to their size in each cell dimension. Electronic minimization energy cutoffs were set to 1×10^{-5} eV. Atom positions, cell shape, and cell size were all allowed to change during geometry minimization. Geometry was minimized with respect to cell stress and was set to a cutoff value of -1×10^{-4} eV in VASP.

Configurations used to calculate cluster expansions were generated until cross-validation scores of less than 0.25 eV or a minimum of 25 configurations were calculated.

Magnetic disordering temperatures were determined from identifying peaks in energy variance vs. temperature plots using the Alloy Theoretical Automated Toolkit (ATAT) Monte Carlo implementation 'emc2'.(van de Walle & Asta (2002)) All simulations were performed with an enclosed radius of 40 Å, resulting in system sizes of $\approx$ 37000 metal ions. Systems were initiated in random configurations, and stepped down in temperature steps of 1 K.

Phase boundary tracing was performed using the ATAT Monte Carlo implementation 'phb'.(van de Walle & Asta (2002)) All systems were again performed with a enclosed radius of 40 Å. Phase boundaries were traced between stable phases identified from cluster expansions at temperature increments of 10K.

The quaternary solid-solution phase boundary cannot be determined through the phase boundary tracer, as this method is implemented for binary systems only. Instead, the system was scanned over regions of chemical

potentials and temperatures, beginning from the high temperature disordered state for a given potential. The ATAT multi-component Monte Carlo implementation 'memc2'(van de Walle & Asta (2002)) was used to perform the determination of the composition as a function of decreasing temperature at a constant chemical potential. Again, an enclosed radius of 40 Å was used, and temperature steps of 10K. Phase boundaries were identified through "memc2" phase boundary detection algorithms.

Results and Discussion

Properties of Eskolaite and Hematite

Both eskolaite and hematite are experimentally known to be high spin and anti-ferromagnetic at low temperatures.(Foner (1963); Searle & Dean (1970)) Hematite is known to have a Morin transition(Morin (1950)) at 250 K, where canting of the magnetic moments causes a net ferromagnetic moment. However, the magnetic moments overall retain their AF alternation within the 4 cation primitive cell, and remain orientated along the easy axis until disordering at hematite's Nèel temperature at 953 K.

To confirm the correct ground state magneto-crystalline configurations can be accurately captured by cluster expansion methods, a series of cluster expansions were performed for both systems for a range of U values. The properties of the lowest energy magnetic configurations from these Cluster Expansions were then examined and tabulated for the different values of U.

The eskolaite system magnetic structure is well behaved throughout all U values and maintains the initial magnetic configuration after geometry relaxation for all tested structures. The resulting cross-validation scores are all < 0.005 eV, well below the recommended value of 0.25 eV,(van de Walle (2019)) ensuring good predicted energies of new configurations. The cross-validation scores and figures of the predicted energies vs. calculated energies can be found in the Supplementary Information for all systems. In contrast, the hematite magnetic structure is highly sensitive to the U parameter. As noted in prior computational work,(Rollmann et al. (2004)) the U parameter for hematite greatly affects the cell volume, causing changes in the balance between the Crystal Field Energy (CFE) and the pairing energy. With no correction, the lattice volume is highly reduced, raising the CFE, making the low spin configuration more favorable. For U = 0 eV this system is highly unstable upon application of a Cluster Expansion, and often does not retain its magnetic structure upon geometry relaxation. While a CE fit was ultimately achieved for U = 0 eV, the overall CV score was poor. For U = 1 eV, not enough stable configurations could be made to produce a valid cluster expansion. Starting at U equal to 2 eV however, the high spin configuration is adopted, and magnetic configurations become much more stable. Cluster Expansions for systems with $U \geq 2$ eV retain their magnetic configurations upon

geometry relaxations and result in low cross-validation scores, < 0.005 eV, in line with those from the eskolaite systems.

For both the eskolaite and hematite systems, the major contributions to the total energy are given by identical sets of pair cluster ECIs as illustrated in Fig. 2. The multiplicity and distances of these pairs on the initial lattice geometry are given in Table 1. The ECI pair energies were plotted in the top figures of Fig. 3 as function of U and indicate decreasing interaction strengths with increasing U. The strongest interactions are positive, indicating energetic favorability of anti-ferromagnetism for both systems. As the interaction strengths are decreasing with U, it may be predicted that this parameter will ultimately affect the magnetic interaction strengths of these metals within a mixture of aluminum. This effect can be seen by examining the shifts in the predicted magnetic disordering temperature of these systems across U. As U increases, the calculated magnetic disordering temperature decreases. This may provide a method to "tune" U to give the correct disordering temperature.

For eskolaite the two primary interactions are from ECI1 and ECI2 (Figure 2). These correspond to a direct exchange interaction between t_{2g} orbitals of the shorter metal-metal bonds across edge sharing octahedra. For hematite, the two primary interactions are instead ECI3 and ECI4. These correspond to a superexchange interaction between e_g orbitals of the metal ions across the p orbitals of oxygens across corner sharing octahedra.

The bottom figures of Fig. 3 show the magnetic interaction parameters J corresponding to each ECI. Details of this conversion are found in the SI. Note that while for this case, ECI's were able to be converted to J parameters, this is only possible for 2-component cluster expansions with a maximum of 2-body clusters, and uniform spin values at each magnetic atom site. While useful for comparison to experimental data, and determination of good U parameters, better energetic predictions of magnetic configurations may rely on inclusion of n-body clusters. ECI's derived from the full multi-component, n-body cluster expansion would be more accurate in final construction of phase diagrams.

These parameters were compared to experimental values derived from neutron scattering dataSamuelsen et al. (1970); Samuelsen & Shirane (1970) and those from other computational workShi et al. (2009); Nabi et al. (2010) that fit these parameters to sets of calculated magnetic configuration energies. Data for these figures are listed in Table 2. As ECIs and experimental J values were ordered by increasing distance, the labeling is equivalent. The experimental data has been scaled by a factor of two to account for the fitted Heisenberg Hamiltonian used in these models not including a common leading 1/2 term. For eskoalite, the U = 1 eV gave reasonable agreement with experiment, though it shows more significant contributions from the J3 and J4. For hematite, the U = 5 eV matches very closely with experiment, though identifies J1 as being negative. The computational models are not directly comparable, but should give reasonably similar results.

For comparison, two prior works were cited using values generated from Hubbard parameters similar to those used in this study. The eskolaite prior computational work was fit to a cluster expansion of 12 configurations only, and the reported ECI values were converted to J values here showing good agreement. The hematite study was fit directly to the Heisenberg Hamiltonian, and its values are reported here without conversion. Note that in this study, J3 was reported as two degenerate sets of J values, J3 and J4, thereby shifting the higher J parameters up in index by one. They have been renumbered here to match the order from the experimental data, and the resulting comparison shows good agreement with these calculations.

For all values of U for eskolaite, and for U $\geq$ 2 for hematite, the same lowest energy AFM magnetic configurations were found, and are pictured in Fig. 4. These lowest energy magneto-crystalline structures were found to be of the same size as the primitive cell, with no symmetry breaking magnetic interactions. The magnetic ordering difference between each system is a result of the primarily direct exchange interactions of eskolaite and the primarily superexchange interactions of hematite resulting in + - + - and + + - - configurations respectively. These results are in line with prior computational work identifying these as the lowest energy primitive cell configurations.(Shi et al. (2009); Rollmann et al. (2004)) Additionally, based on the size of the energy gaps between the FM and AFM configurations, we predict that magnetic contributions will have more significant effect on the corundum:hematite phase diagram.

The crystal properties of these systems as well as the aluminum corundum system were tabulated for the lowest energy configurations for different values of U in Table 3. The most notable result is that for both systems, an increasing U parameter results in moving further from the experimental cohesive energy value. For eskolaite, this presents little issue, as all calculated parameters trend towards the experimental value with decreasing U and are close to these values with DFT+U correction. But this does present an issue for hematite, as the magnetic properties are only properly captured at U $\geq$ 2.

Configurational Phase Boundary of Corundum-Eskolaite and Corundum-Hematite

In the simplest approximation of a metal-metal solid oxide solution, the magnetic metal is approximated with zero magnetic degrees of freedom, and is fixed to a single orientation. This requires a new set of Cluster Expansions to be performed for the $xM1_2(1\text{-}x)M2_2O_3$ systems. For eskolaite, the two metal components are Al and Cr, and for hematite, Al and Fe. In these binary systems, the phase diagram can be determined through matching of the chemical potentials for each ground state using the Monte Carlo "phb" method from ATAT. The resulting phase diagram, shown in Fig. 5, for the corundum eskolaite system well approximates the experimental phase diagram, but the boundary becomes more reduced in temperature with increasing U. Notably, there is an initial large reduction in the phase boundary, with the shift seeming to converge with

increasing U. It should also be commented that the disconnected portions of the calculated phase boundary are due to the increasingly smaller temperature steps required to sample this region, and are not due to an absence of a phase boundary.

The phase diagram for the corundum hematite system is only slightly more complex than the eskolaite mixture with inclusion of an additional ground state identified from DFT calculations of configurations used to create the cluster expansion. It should first be noted that experimental phase diagrams have not reported the existence of this state, but also have never reported a closed solvus in the literature that the authors are aware of. The result of these calculations is the prediction of a new stable phase composed of equal amounts Fe(III) and Al(III), pictured in the phase diagram in Fig. 5, and having ferromagnetic ordering. This prediction is based off *ab-initio* calculations of ground state configurations only, and do not include zero point energy vibrational contributions.

The higher values of U follow a similar pattern to those in the Al:Cr system, where increasing U leads to decreased gaps in the mixing energy, and a lowered phase boundary, though the shift is less drastic. The intermediate stable $Al_2Fe_2O_6$ phase is identified as a ground state for all values of U. Overall the calculated phase boundary is much further from the experimental values when only accounting for the configurational energies and is likely due to the missing magnetic contributions. Additionally, as increasing U decreases the cohesive energy of hematite, starting at U = 2 eV may be leading to lower phase boundary temperatures.

Configurational and Magnetic Contributions to Phase Boundary of Corundum-Eskolaite and Corundum-Hematite

To determine the magnetic contributions to the phase boundary, each system was modeled using a 4-component cluster expansion in order to include configurational and magnetic terms simultaneously. For the corundum:eskolaite system, this consisted of a series of labeled chemical components Cr1,Cr2,Al3,Al4. Here the Cr1 is a chromium(III) with an 'up' magnetic moment, and the Cr2 is a 'down' magnetic moment. The aluminum components lack a magnetic moment, but are separated into two identical Cluster Expansion components in order to yield the correct compositional high temperature statistics.

The phase diagrams generated from this are quaternary, but can be simplified by combining the aluminum components and the magnetic components to form a binary phase diagram. This will mean that the magnetization axis is "hidden". While it is possible to map out the magnetic phase diagram in conjunction with the atomic configuration diagram, the focus of this work is on shifts to the latter upon the inclusion of magnetism. The following diagrams represent the anti-ferromagnetic and disordered region of the magnetization axis, i.e. equal parts up and down magnetic moments.

Within the corundum-eskolaite system, Fig. 6, it can be seen that there is very little change in the phase diagram in the aluminum rich region. On the chromium rich side, for U = 0 eV, there is a noticeable shift upwards in the phase boundary, and slight shifts downwards at U $>$ 0. This is likely due to the presences of the artificially high magnetic disordering temperature occurring right at the region for the expected corundum:eskolaite phase transition. Overall however, there is very little difference upon inclusion of magnetic degrees of freedom into this system, and a ferromagnetic treatment of chromium ions gives good agreement with experiment. This might be predicted as the magnetic disordering temperature of eskolaite is 309K, intersecting the miscibility gap with corundum at a comparatively low temperature.

For the corundum:hematite system, the $Fe_2Al_2O_6$ was again determined to be a ground state for all values of U. As it is ferromagnetic, it was omitted from the final binary phase diagram. The inclusion of the magnetic terms for this system resulted in a drastic shift to the phase diagram. For U = 2 eV, the miscibility gap has greatly increased, and the phase boundaries are very well aligned with the experimental data. For increasing U the phase boundary decreases, but even at it's lowest value at U = 5 eV, it is still closer to experiment than the purely configurational calculated phase boundary. For all values of U, the calculated magnetic disordering temperature is well above the boundary for the calculated miscibility gap between Al and Fe. As the magnetic disordering temperature for hematite occurs at 905K, it should normally intersect the miscibility gap with corundum. The presented model therefore does not represent the physical system completely, but is clearly able to capture more accurate mixing properties.

Ultimately, the magnetic interactions for some systems are strong enough to require consideration when constructing phase diagrams, though it may not be clear from the outset how significant the changes to critical disordering temperatures may be.

Implications

Magnetic contributions may have a significant impact on material phase boundaries, but present an exceptional challenge to incorporate accurately into an already immense configurational space. By inclusion of an Ising-like model of magnetism into the configurational portion of a multi-component cluster expansion, it is at least possible to simultaneously capture this simplified magnetic model in conjunction with atomic configurations. Future work would benefit from inclusion of Heisenberg-like interactions as part of the Monte Carlo finite temperature calculations which allow for rotation of magnetic moments in addition to swapping of atomic sites.

While for the corundum-eskolaite system, where it may be expected that the weaker magnetic pair interac-

tions would result in little noticeable effect and negligible changes to phase diagram calculation were present, for corundum-hematite, inclusion of magnetic degrees of freedom is absolutely essential for reproducing experimental results. These results show the necessity of incorporating magnetism into phase equilibria for systems in which strong magnetic pair interactions are present.

Acknowledgements

This research was supported by IDREAM (Interfacial Dynamics in Radioactive Environments and Materials), an Energy Frontier Research Center funded by the U.S. Department of Energy (DOE), Office of Science, Basic Energy Sciences (BES). Computational work was performed using the Washington State University Center for Institutional Research Computing, and the Institutional Computing facility at Pacific Northwest National Laboratory (PNNL). PNNL is a multi-program national laboratory operated for DOE by Battelle Memorial Institute under Contract DE-AC05-76RL0-1830.

Tables

Table 1: Effective cluster interaction (ECI) distances with respect to cluster expansion parent lattice dimensions.

ECI	multiplicity	distance (Å)
1	2	2.65
2	6	2.78
3	6	3.50
4	12	3.84
5	2	4.76

This is the peer-reviewed, final accepted version for American Mineralogist, published by the Mineralogical Society of America.
The published version is subject to change. Cite as Authors (Year) Title. American Mineralogist, in press.
DOI: https://doi.org/10.2138/am-2022-8584. http://www.minsocam.org/

Table 2: Calculated magnetic exchange energies (J) as compared to experiment and prior computational work.

J (K)	1	2	3	4	5
Cr_2O_3					
U = 0 eV	-202	-167	21.9	35.6	-12.8
U = 1 eV	-125	-103	31.8	40.0	2.73
U = 2 eV	-68.1	-66.8	30.5	40.0	-11.4
U = 3 eV	-53.0	-48.6	35.1	38.9	-0.885
Exp.[a]	-174.6	-75.6	1.4	0.4	-4.4
Comp.[b]	-147	-107	7.80	14.6	-23.0
Fe_2O_3					
U = 2 eV	0.127	-22.2	-162	-94.7	-41.9
U = 3 eV	-13.2	-22.0	-127	-80.6	6.47
U = 4 eV	-4.27	-6.76	-88.6	-67.6	-4.38
U = 5 eV	-9.65	-3.02	-71.1	-57.8	-3.69
Exp.[c]	12	3.2	-59.4	-46.4	-2.
Comp.[d]	-15.9	-6.3	-72.1	-50.1	-9.

[a] Samuelsen et al. (1970)
[b] Shi et al. (2009) LDSA+U U-J = 2.42 eV
[c] Samuelsen & Shirane (1970)
[d] Nabi et al. (2010) GGA+U U-J = 5 eV

Table 3: Lattice properties of corundum, eskolaite, and hematite. Properties of magnetic structures were derived from their ground-state AFM magneto-crystalline configurations

	a	α	V	mag. mom.	CohE	Δ E FM/AFM	Nèel/Curie
	(Å)	(deg)	(Å^3)	(μ_B)	(kJ/mol/f.u.)	(meV)	(K)
Al_2O_3							
Exp.[a]	5.12	55.28	84.5				
	5.18	55.30	87.6				
Cr_2O_3							
Exp.	5.35[b]	55.0[b]	95.7[b]	2.48[c], 2.76[d]	2679[e]		309[f]
U = 0 eV	5.42	54.2	97.3	2.69	2582	106	1090
U = 1 eV	5.36	56.3	99.8	2.81	2505	56.1	790
U = 2 eV	5.39	56.2	100.8	2.88	2433	32.1	600
U = 3 eV	5.41	56.1	101.9	2.94	2365	15.0	410
Fe_2O_3							
Exp.	5.43[a]	55.3[a]	100.8[a]		2403[e]		953 [g]
U = 0 eV	5.42	54.3	97.56	0.98	2427		
U = 2 eV	5.47	55.0	102.5	3.95	2359	397	3130
U = 3 eV	5.48	55.0	102.9	4.06	2312	323	2520
U = 4 eV	5.47	55.1	102.9	4.14		265	2230
U = 5 eV	5.47	55.1	102.7	4.43		219	1822

[a] Pauling & Hendricks (1925)
[b] Zachariasen (1928)
[c] Brown et al. (2002)
[d] Corliss et al. (1965)
[e] Glasser & Sheppard (2016)
[f] Brockhouse (1953)
[g] De Boer & Dekkers (1998)

340

Figures

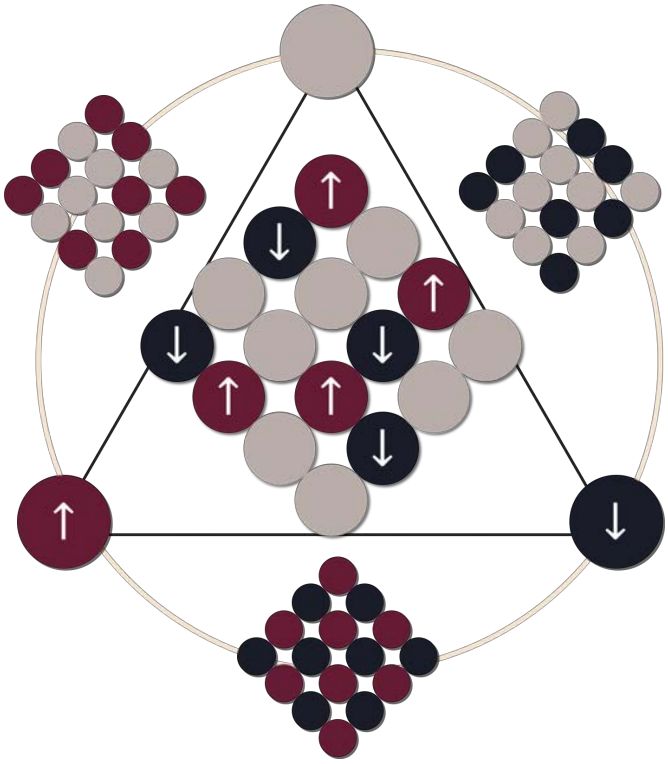

Figure 1: Ternary phase diagram of atomic and magnetic configurational components.

This is the peer-reviewed, final accepted version for American Mineralogist, published by the Mineralogical Society of America.
The published version is subject to change. Cite as Authors (Year) Title. American Mineralogist, in press.
DOI: https://doi.org/10.2138/am-2022-8584. http://www.minsocam.org/

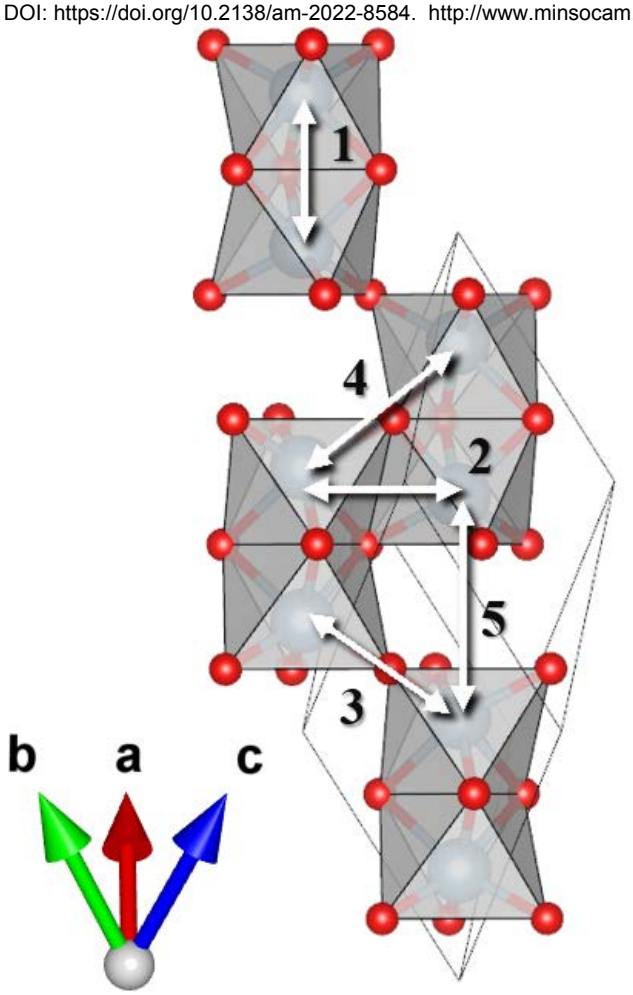

Figure 2: Effective cluster interactions of eskolaite and hematite.

This is the peer-reviewed, final accepted version for American Mineralogist, published by the Mineralogical Society of America.
The published version is subject to change. Cite as Authors (Year) Title. American Mineralogist, in press.
DOI: https://doi.org/10.2138/am-2022-8584. http://www.minsocam.org/

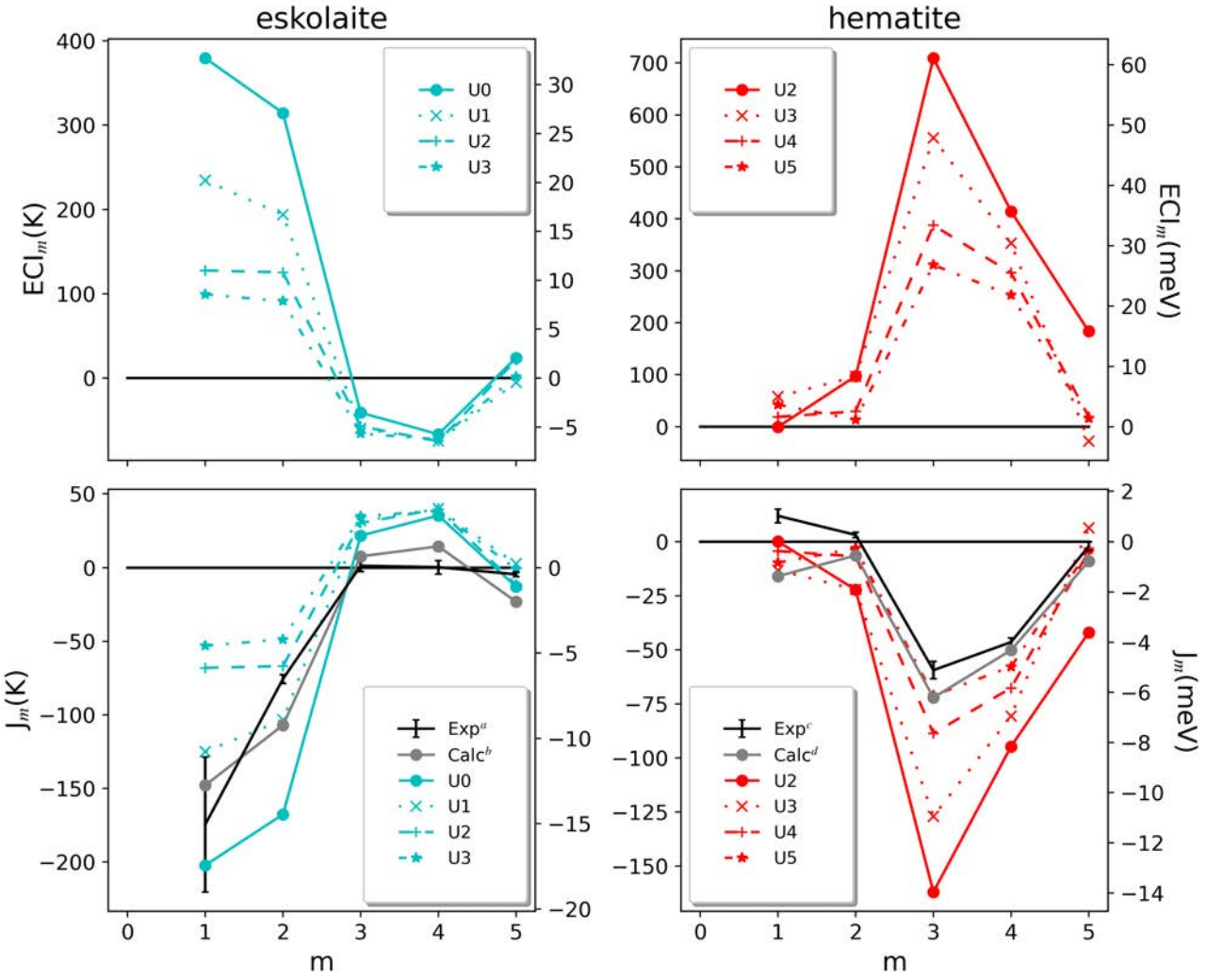

Figure 3: Top: Variation in the magnitude of effective cluster interaction (ECI) values of eskolaite and hematite calculated over a range of GGA+U values. The ECI values here correspond with those shown in Figure 2. Bottom: ECI's have been converted to magnetic exchange terms J for comparison to experimental estimates and values obtained from prior computational work.

[a] Samuelsen et al. (1970)

[b] Shi et al. (2009) LDSA+U U-J = 2.42 eV

[c] Samuelsen & Shirane (1970)

[d] Nabi et al. (2010) GGA+U U-J = 5 eV

This is the peer-reviewed, final accepted version for American Mineralogist, published by the Mineralogical Society of America.
The published version is subject to change. Cite as Authors (Year) Title. American Mineralogist, in press.
DOI: https://doi.org/10.2138/am-2022-8584. http://www.minsocam.org/

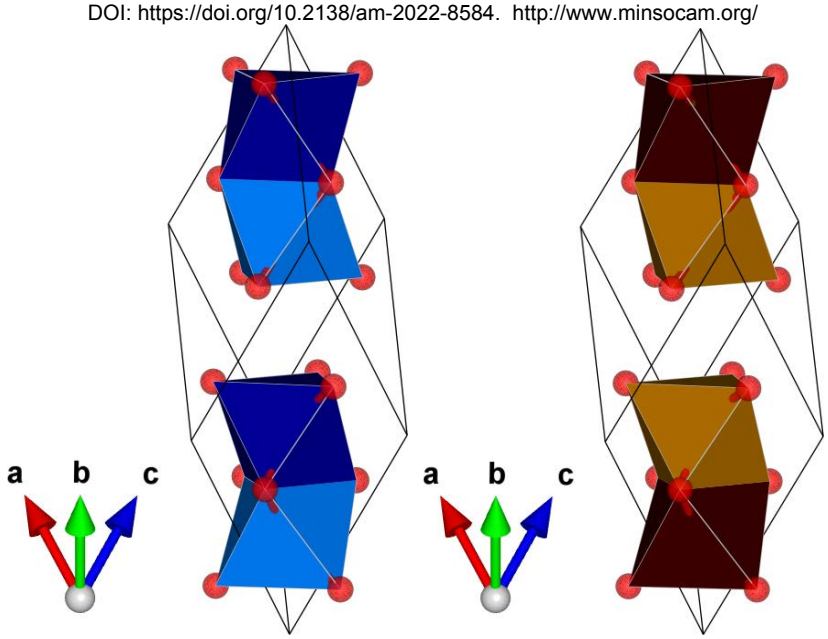

(a) eskolaite anti-ferromagnetic structure (b) hematite anti-ferromagnetic structure

Figure 4: Magneto-crystalline structures computed for eskolaite and hematite. The lighter and darker color polyhedra represent the opposing directions of the magnetic moments.

This is the peer-reviewed, final accepted version for American Mineralogist, published by the Mineralogical Society of America.
The published version is subject to change. Cite as Authors (Year) Title. American Mineralogist, in press.
DOI: https://doi.org/10.2138/am-2022-8584. http://www.minsocam.org/

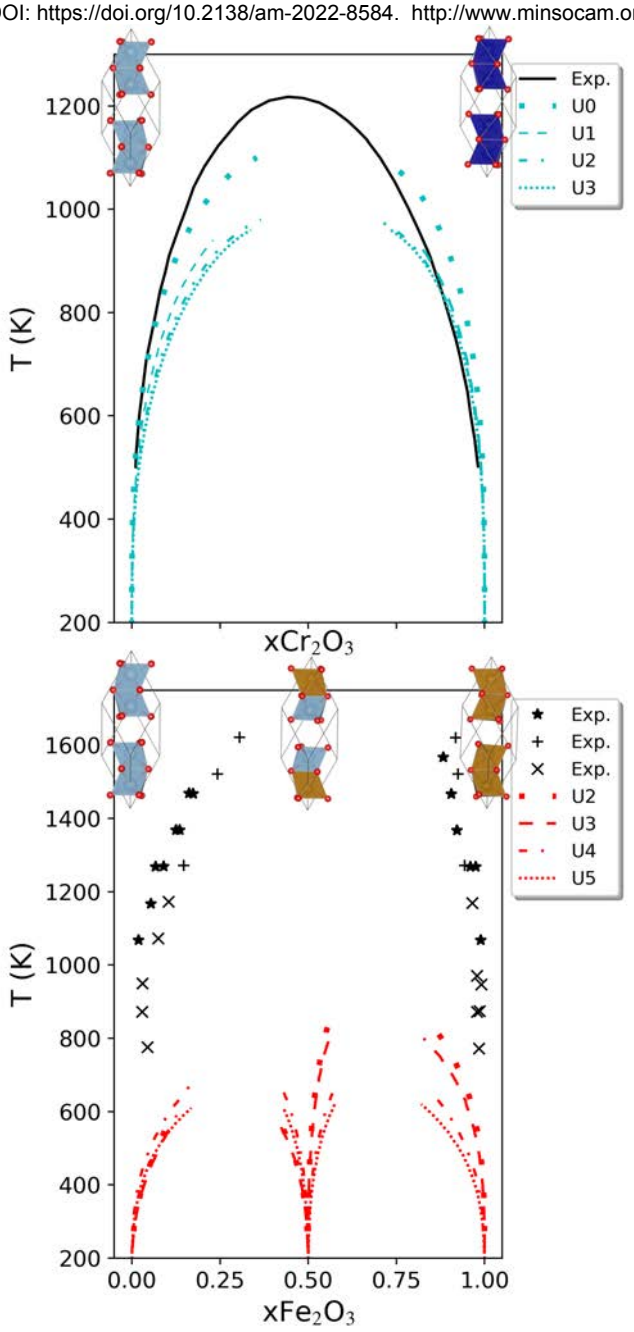

Figure 5: Calculated phase boundary of (Top) Al_2O_3 and ferromagnetic Cr_2O_3 and (Bottom) Al_2O_3 and ferromagnetic Fe_2O_3 across values of U vs. the experimental curve.(Chatterjee et al. (1982)) Ground state structures are pictured at the top of each plot.

This is the peer-reviewed, final accepted version for American Mineralogist, published by the Mineralogical Society of America.
The published version is subject to change. Cite as Authors (Year) Title. American Mineralogist, in press.
DOI: https://doi.org/10.2138/am-2022-8584. http://www.minsocam.org/

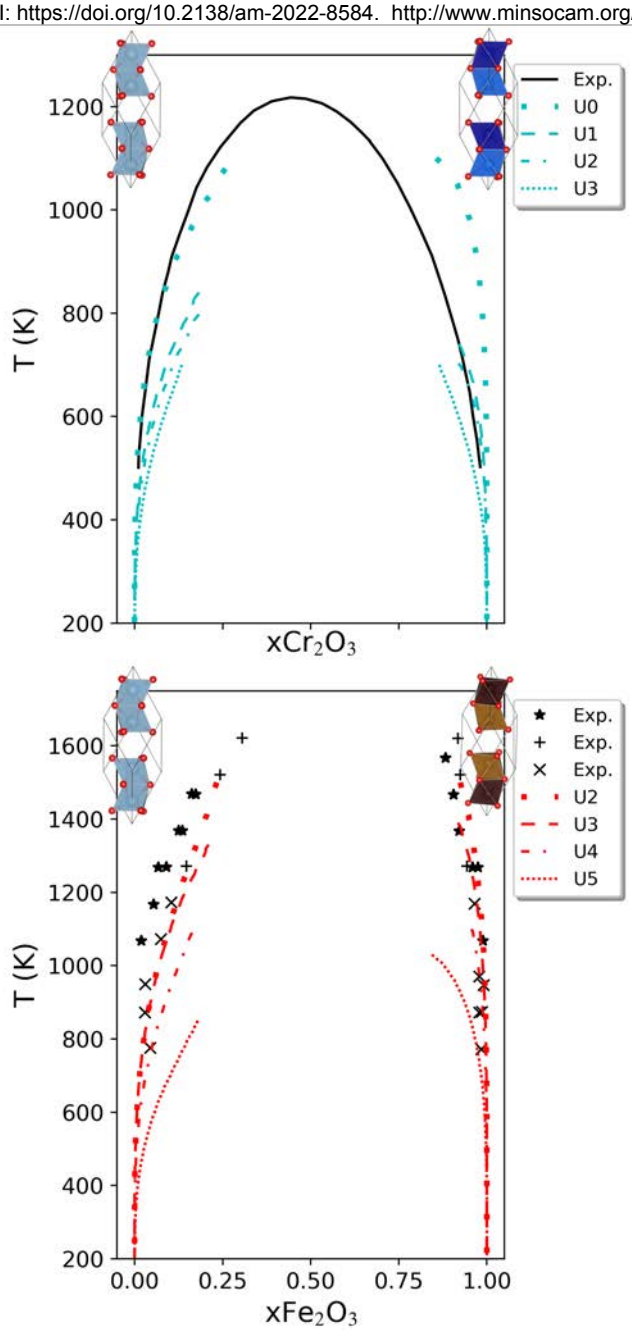

Figure 6: Calculated phase boundary of (top) Al_2O_3 and anti-ferromagnetic Cr_2O_3 and (bottom) Al_2O_3 and anti-ferromagnetic Fe_2O_3 across values of U vs. the experimental curve. Ground state structures are pictured at the top of each plot.

References

Atlas, L., & Sumida, W. (1958). Solidus, subsolidus, and subdissociation phase equilibria in the system Fe-Al-O. *Journal of the American Ceramic Society*, *41*(5), 150–160.

Borisov, P., Hochstrat, A., Chen, X., Kleemann, W., & Binek, C. (2005). Magnetoelectric switching of exchange bias. *Physical Review Letters*, *94*(11), 117203.

Brockhouse, B. N. (1953). Antiferromagnetic structure in Cr_2O_3. *The Journal of Chemical Physics*, *21*(5), 961–962.

Brown, P., Forsyth, J., Lelièvre-Berna, E., & Tasset, F. (2002). Determination of the magnetization distribution in Cr_2O_3 using spherical neutron polarimetry. *Journal of Physics: Condensed Matter*, *14*(8), 1957.

Burton, B. P. (1991). The interplay of chemical and magnetic ordering. *Reviews in Mineralogy and Geochemistry*, *25*(1), 303–322.

Chatterjee, N. D., Leistner, H., Terhart, L., Abraham, K., & Klaska, R. (1982). Thermodynamic mixing properties of corundum–eskolaite, α-$(Al,Cr^{3+})_2O_3$, crystalline solutions at high temperatures and pressures. *American Mineralogist*, *67*(7-8), 725–735.

Chatterjee, S., Conroy, M. A., Smith, F. N., Jung, H.-J., Wang, Z., Peterson, R. A., Huq, A., Burtt, D. G., Ilton, E. S., & Buck, E. C. (2016). Can Cr (III) substitute for Al (III) in the structure of boehmite? *The Royal Society of Chemistry Advances*, *6*(109), 107628–107637.

Corliss, L., Hastings, J., Nathans, R., & Shirane, G. (1965). Magnetic structure of Cr_2O_3. *Journal of Applied Physics*, *36*(3), 1099–1100.

De Boer, C. B., & Dekkers, M. J. (1998). Thermomagnetic behaviour of haematite and goethite as a function of grain size in various non-saturating magnetic fields. *Geophysical Journal International*, *133*(3), 541–552.

Dudarev, S., Botton, G., Savrasov, S., Humphreys, C., & Sutton, A. (1998). Electron-energy-loss spectra and the structural stability of nickel oxide: An lsda+ u study. *Physical Review B*, *57*(3), 1505.

Eremin, N., Talis, R., & Urusov, V. (2008). Computer modeling of the local structure, mixing properties, and stability of binary oxide solid solutions with corundum structure. *Crystallography Reports*, *53*(5), 755–763.

Feenstra, A., Sämann, S., & Wunder, B. (2005). An experimental study of Fe–Al solubility in the system corundum–hematite up to 40 kbar and 1300 C. *Journal of Petrology*, *46*(9), 1881–1892.

Foner, S. (1963). High-field antiferromagnetic resonance in Cr_2O_3. *Physical Review*, *130*(1), 183.

Francis, G., & Payne, M. (1990). Finite basis set corrections to total energy pseudopotential calculations. *Journal of Physics: Condensed Matter*, *2*(19), 4395.

Garrity, K. F. (2019). Combined cluster and atomic displacement expansion for solid solutions and magnetism. *Physical Review B*, *99*(17), 174108.

Glasser, L., & Sheppard, D. A. (2016). Cohesive energies and enthalpies: complexities, confusions, and corrections. *Inorganic chemistry*, *55*(14), 7103–7110.

He, X., Wang, Y., Wu, N., Caruso, A. N., Vescovo, E., Belashchenko, K. D., Dowben, P. A., & Binek, C. (2010). Robust isothermal electric control of exchange bias at room temperature. *Nature materials*, *9*(7), 579–585.

Jacob, K. (1978). Electrochemical determination of activities in Cr_2O_3 Al_2O_3 solid solutions. *Journal of the Electrochemical Society*, *125*, 175–179.

Khan, U., Akbar, A., Yousaf, H., Riaz, S., & Naseem, S. (2015). Ferromagnetic properties of Al-doped Fe_2O_3 thin films by sol-gel. *Materials Today: Proceedings*, *2*(10), 5415–5420.

Kresse, G., & Furthmüller, J. (1996). *Physical Review B*, *54*(16), 11169.

Kresse, G., & Joubert, D. (1999). *Physical Review B*, *59*(3), 1758.

Lavrentiev, M. Y., Nguyen-Manh, D., & Dudarev, S. (2010). Magnetic cluster expansion model for bcc-fcc transitions in Fe and Fe−Cr alloys. *Physical Review B*, *81*(18), 184202.

Morin, F. (1950). Magnetic susceptibility of αFe_2O_3 and αFe_2O_3 with added titanium. *Physical Review*, *78*(6), 819.

Nabi, H. S., Harrison, R. J., & Pentcheva, R. (2010). Magnetic coupling parameters at an oxide-oxide interface from first principles: Fe_2O_3−$FeTiO_3$. *Physical Review B*, *81*(21), 214432.

Pack, J. D., & Monkhorst, H. J. (1977). *Physical Review B*, *16*(4), 1748.

Pattanayak, N., Panda, P., & Parida, S. (2021). Al doped hematite nanoplates: Structural and raman investigation. *Ceramics International*.

Pauling, L., & Hendricks, S. B. (1925). The crystal structures of hematite and corundum. *Journal of the American Chemical Society*, *47*(3), 781–790.

Perdew, J. P., Burke, K., & Ernzerhof, M. (1996). *Physical Review Letters*, *77*(18), 3865.

Pinney, N., Kubicki, J. D., Middlemiss, D. S., Grey, C. P., & Morgan, D. (2009). Density functional theory study of ferrihydrite and related Fe-oxyhydroxides. *Chemistry of Materials*, *21*(24), 5727–5742.

Rollmann, G., Rohrbach, A., Entel, P., & Hafner, J. (2004). First-principles calculation of the structure and magnetic phases of hematite. *Physical Review B*, *69*(16), 165107.

Samuelsen, E., Hutchings, M., & Shirane, G. (1970). Inelastic neutron scattering investigation of spin waves and magnetic interactions in Cr_2O_3. *Physica*, *48*(1), 13–42.

Samuelsen, E., & Shirane, G. (1970). Inelastic neutron scattering investigation of spin waves and magnetic interactions in α-Fe_2O_3. *physica status solidi (b)*, *42*(1), 241–256.

Sanchez, J. M., Ducastelle, F., & Gratias, D. (1984). Generalized cluster description of multicomponent systems. *Physica A: Statistical Mechanics and its Applications*, *128*(1-2), 334–350.

Searle, C., & Dean, G. (1970). Temperature and field dependence of the weak ferromagnetic moment of hematite. *Physical Review B*, *1*(11), 4337.

Shi, S., Wysocki, A. L., & Belashchenko, K. D. (2009). Magnetism of chromia from first-principles calculations. *Physical Review B*, *79*(10), 104404.

Sitte, W. (1985). Investigation of the miscibility gap of the system chromia-alumina below 1300 C. *Materials Science Monographs*, *28*, 451–456.

Turnock, A., & Eugster, H. (1962). Fe—Al oxides: phase relationships below 1,000 C. *Journal of Petrology*, *3*(3), 533–565.

Van De Walle, A. (2009). Multicomponent multisublattice alloys, nonconfigurational entropy and other additions to the Alloy Theoretic Automated Toolkit. *Calphad*, *33*(2), 266–278.

van de Walle, A. (2019). The alloy-theoretic automated toolkit (ATAT): A user guide.

van de Walle, A., & Asta, M. (2002). *Modeling and Simulation in Materials Science and Engineering*, *10*(5), 521.

Zachariasen, W. (1928). Untersuchungen über die kristallstruktur von sesquioxyden und verbindungen ABO_3. *Skrifter utgitt av det Norske Videnskaps-Akademi i Oslo*, *1*, 1–165.